IOPscience iopscience.iop.org

Home Search Collections Journals About Contact us My IOPscience

Alignment sensing and control in advanced LIGO

This content has been downloaded from IOPscience. Please scroll down to see the full text.

2010 Class. Quantum Grav. 27 084026

(http://iopscience.iop.org/0264-9381/27/8/084026)

View the table of contents for this issue, or go to the journal homepage for more

Download details:

IP Address: 128.230.139.221
This content was downloaded on 22/06/2017 at 21:11

Please note that terms and conditions apply.

You may also be interested in:

Advanced Virgo: a second-generation interferometric gravitational wave detector
F Acernese, M Agathos, K Agatsuma et al.

Status of LIGO at the start of the fifth science run
Samuel J Waldman and the LIGO Science Collaboration

Length sensing and control strategies for the LCGT interferometer
Y Aso, K Somiya and O Miyakawa

Advanced LIGO: the next generation of gravitational wave detectors
Gregory M Harry and the LIGO Scientific Collaboration

Novel sensing and control schemes for a three-mirror coupled cavity
S H Huttner, B W Barr, M V Plissi et al.

Advanced LIGO: length sensing and control in a dual recycled interferometric gravitational wave antenna
Kiwamu Izumi and Daniel Sigg

Seismic isolation of Advanced LIGO: Review of strategy, instrumentation and performance
F Matichard, B Lantz, R Mittleman et al.

Advanced LIGO optical configuration and prototyping effort
Alan Weinstein

Virgo: a laser interferometer to detect gravitational waves
T Accadia, F Acernese, M Alshourbagy et al.

IOP PUBLISHING CLASSICAL AND QUANTUM GRAVITY

Class. Quantum Grav. **27** (2010) 084026 (15pp) doi:10.1088/0264-9381/27/8/084026

Alignment sensing and control in advanced LIGO

L Barsotti, M Evans and P Fritschel

Massachusetts Institute of Technology, Cambridge, MA 02139, USA

E-mail: lisabar@ligo.mit.edu

Received 14 November 2009, in final form 8 February 2010
Published 6 April 2010
Online at stacks.iop.org/CQG/27/084026

Abstract

The advanced LIGO detectors are currently in their final design stage, and the installation phase will start at the end of 2010: they will have about 10 times better sensitivity than initial LIGO, with a sensitive band ranging from 10 Hz to 10 kHz. As compared with previous LIGO detectors, there will be increased complexity in the optical configuration, improved seismic isolation system and significantly higher power circulating in the arm cavities. In the new detectors, the control of the angular orientation of the mirrors will be particularly challenging. The advanced LIGO (aLIGO) mirrors need to have a residual angular motion of the order of 1 nrad RMS in order to achieve high sensitivity. In the high power regime, the torque induced by radiation pressure effects will be comparable with the restoring torque of the mirror suspension, such that we must think of the opto-mechanical response, instead of just the mechanical response. These modifications have to be considered in order to design the control strategy for keeping the mirrors well aligned. Moreover, to meet the sensitivity target the alignment control noise coupled to the gravitational-wave channel must be well below 6×10^{-18} m/$\sqrt{\text{Hz}}$ at 10 Hz. We developed a model of the alignment sensing and control scheme of aLIGO which takes into account radiation pressure effects and meets the noise target.

PACS numbers: 04.80.Nn, 95.55.Ym, 95.75.Kk

(Some figures in this article are in colour only in the electronic version)

1. Introduction

The first generation of gravitational-wave interferometric detectors (LIGO [1], VIRGO [2], GEO [3]) will be replaced with second generation instruments in the next few years. Current estimates predict that the improved sensitivity will allow for detections of gravitational waves at the rate of a few tens of events per year [4]. Advanced LIGO (aLIGO) is designed to beat the LIGO sensitivity by about a factor of 10 broadband, and it will push the lowest frequency detectable from 40 Hz down to 10 Hz.

 © 2010 IOP Publishing Ltd Printed in the UK & the USA

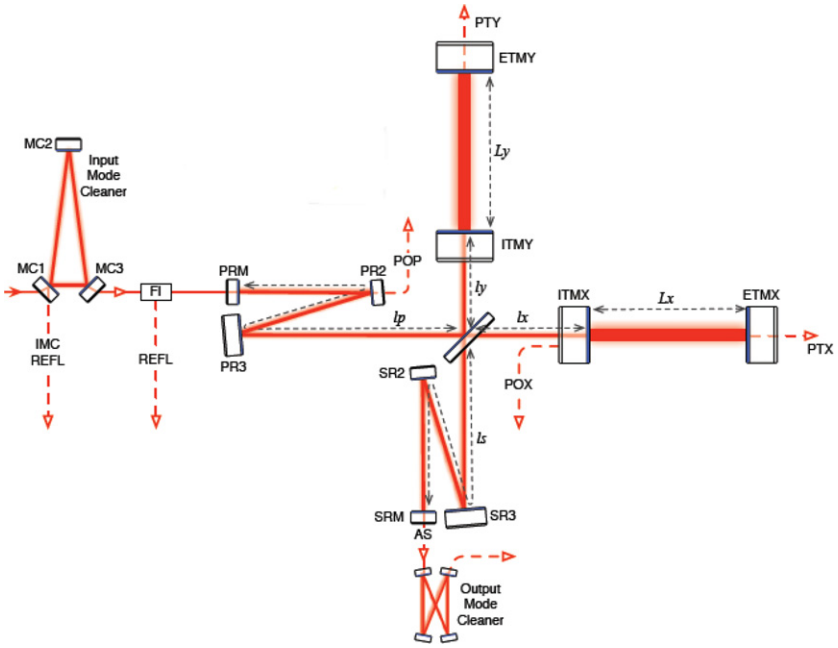

Figure 1. The advanced LIGO optical layout [7]. Together with the test masses (ITMX, ITMY, ETMX, and ETMY), and the beam splitter (BS), there are six other main optics: the power recycling mirror (PRM), the power recycling cavity telescope (PR2 and PR3), the signal recycling mirror (SRM) and the associated telescope mirrors (SR2 and SR3). The optical parameters are listed in appendix A.

The main features of aLIGO are

- about 10 times higher input laser power than LIGO[1];
- an optical layout which includes stable recycling cavities and a signal recycling mirror (see figure 1);
- complex suspensions and seismic isolation systems for the main optics.

While these changes will improve the detector performance, they complicate the control strategy needed to keep the interferometer (IFO) at its operating point. All the mirrors need to be well aligned both in pitch (a rotation of the mirror about the horizontal axis) and yaw (a rotation of the mirror about its vertical axis) with respect to each other and the incoming beam in order to guarantee stable operation of the detector. Considerations of beam–jitter coupling [5] suggest that the residual angular motion of the test masses in aLIGO needs to be of the order of 1 nrad RMS to meet the sensitivity target. Since the expected angular motion of the aLIGO mirrors under local controls is at least three orders of magnitude higher, a control system is needed to reduce the motion down to the desired level.

An alignment sensing and control scheme (ASC) has operated in LIGO for several years [6]. It uses signals which give the relative angular orientation of the mirrors, extracted at the IFO output ports through quadrant photo detectors (QPDs). Each QPD has four separate elements which allow it to sense the position of the beam impinging upon the diode by

[1] Enhanced LIGO, a platform for testing some of the aLIGO new technology, has been operated with a maximum input power of 20 W during the Scientific Run S6, about 3 times the input power of initial LIGO.

comparing the amount of light present on each quadrant. Moreover, the sensing of angular misalignments is performed through a phase modulation–demodulation technique, known as 'wavefront sensing' (WFS) [6], in which the QPD output signals are demodulated at the modulation frequency to produce alignment signals.

WFS produce alignment signals via the interference between the fundamental TEM_{00} Hermite–Gaussian mode of the carrier (sidebands) and the TEM_{01} and TEM_{10} modes of the sidebands (carrier) generated by the misalignment of the IFO optics. The interference signal depends on the relative Gouy phase between the TEM_{00} and TEM_{10} modes, which is a function of the longitudinal position of the detector along the beam axis. For this reason, angular misalignments of different mirrors can be distinguished by placing detectors at different locations along the optical path.

Both dc and demodulated signals are used in the ASC scheme. They are filtered and fed back to actuators on the mirrors to keep them aligned. At the same time, there is a fundamental requirement at the level of control noise which can be introduced into the system: it must be low enough to be compatible with sciencemode operation, which means that the angular noise coupled to the gravitational-wave channel must be well below the sensitivity of the IFO.

This architecture of the ASC scheme is now standard for interferometric gravitational-wave detectors. However, the increased complexity of aLIGO requires modifications of the ASC scheme in order to take into account the new elements in the design, which can be understood in terms of additional complexity for the ASC:

- radiation pressure effects introduced by the high circulating power inside the arm cavities;
- more mirrors to be controlled, i.e. a new sensing scheme is required for controlling the signal recycling mirror (SRM), and the four telescope mirrors required to make stable recycling cavities;
- a more complex control strategy which takes into account the transfer functions of the multi-stage mirror suspensions;
- more stringent noise requirements, since the angular noise must be compatible with science mode operation down to 10 Hz (instead of 40 Hz as in previous LIGO detectors), where aLIGO aims to have a sensitivity of 6×10^{-18} m $\mathrm{Hz}^{-1/2}$.

A possible ASC scheme that addresses these problems has been developed using the frequency domain tool Optickle [8], which simulates the opto-mechanical transfer functions of the angular degrees of freedom (DOFs) of the IFO.

In section 2, we describe the effects produced by radiation pressure. In particular, we introduce the framework of our model by defining a convenient basis for the DOFs of the IFO. Section 3 shows some of the characteristics of the ASC model: the input noises, the control scheme and the performance, both in terms of the residual angular mirror motion and in terms of noise coupling to the gravitational-wave channel.

2. Radiation pressure effects

The maximum input laser power planned for aLIGO is 125 W. The total power circulating inside the arms when the IFO is operating at maximum power is higher than 700 kW. Under these conditions, the torque induced by radiation pressure is comparable to the restoring torque of the pendulum, and it modifies the opto-mechanical transfer function of the system. For this reason, understanding radiation pressure effects is a fundamental step in the design of an alignment control scheme.

The effects of radiation pressure in a single Fabry–Perot cavity have been studied in [9]. Here, we apply the analysis to the aLIGO arm cavities, and we model the opto-mechanical transfer functions of the system.

2.1. Torsional-stiffness matrix

For a single Fabry-Perot cavity, the radiation pressure torque can be written in terms of the optical parameters of the cavities in the form of a 2×2 matrix which couples the static misalignments of the two cavity mirrors [9]:

$$\tau = \hat{\mathbf{K}}_{\rm opt}(g_{\rm ETM}, g_{\rm ITM}, L, P) \begin{pmatrix} \theta_{\rm ETM} \\ \theta_{\rm ITM} \end{pmatrix}, \tag{1}$$

where $g_{\rm ETM}$ and $g_{\rm ITM}$ are the g factors of the cavity, L is the length and P is the intra-cavity power. $\hat{\mathbf{K}}_{\rm opt}$ is the torsional stiffness matrix defined as

$$\hat{\mathbf{K}}_{\rm opt} = k_0 \begin{pmatrix} g_{\rm ITM} & 1 \\ 1 & g_{\rm ETM} \end{pmatrix} \text{ with } k_0 = \frac{2PL}{c(g_{\rm ETM}g_{\rm ITM} - 1)}. \tag{2}$$

The analytical expressions for the eigenvalues of the torsional stiffness matrix $\hat{\mathbf{K}}_{\rm opt}$ are

$$k_{S,H} = k_0 \frac{(g_{\rm ETM} + g_{\rm ITM}) \pm \sqrt{(g_{\rm ETM} - g_{\rm ITM})^2 + 4}}{2}, \tag{3}$$

where the indices S and H refer to the *soft* and *hard* modes in order to emphasize the fact that in one case the torque induced by radiation pressure tends to make the mode stiffer (hard), while in the other case it tends to make the mode less stiff (soft). In aLIGO, the soft mode has the potential to be unstable, as described in section 2.2. In this case, active feedback is required to stabilize it.

The two eigenvectors relative to the eigenvalues k_S and k_H are

$$v_S = \left[1, \frac{k_0}{k_S - k_0 g_{\rm ETM}}\right] \qquad v_H = \left[\frac{k_0}{k_0 g_{\rm ITM} - k_H}, -1\right]. \tag{4}$$

They correspond to the basis of cavity misalignments that makes the torque stiffness matrix diagonal. This is the normal mode basis that decouples the effects of radiation pressure in two independent modes: 'hard' and 'soft' (see figure 2). In the hard mode, the tilt of the beam axis makes the radiation pressure push the mirrors back to their aligned position. In the soft mode, on the other hand, the shifting beam axis causes the radiation pressure to push the mirrors to larger angles.

2.2. Shift of the pendulum resonance frequency in the aLIGO arm cavities

The angular resonance frequency of the opto-mechanical transfer function of a pendulum (ratio of torque applied on the test mass to angular position of the test mass) is determined by the sum of the suspension restoring torque $k_{\rm res}$ and the radiation pressure torque $k_{\rm opt}$:

$$f_\alpha = \frac{1}{2\pi}\sqrt{\frac{k_{\rm res} + k_{\rm opt}}{I}}, \tag{5}$$

where I is the moment of inertia of the suspension chain. In aLIGO, the mirror is not suspended by a simple pendulum, but by a quadruple pendulum chain. For this reason, the mechanical transfer function is somewhat more complicated. However, this analysis can be considered an approximation of the behavior of the lowest resonance frequency. The parameters of the aLIGO arm cavities needed to compute the resonance frequencies are listed in table 1 and in appendix A.

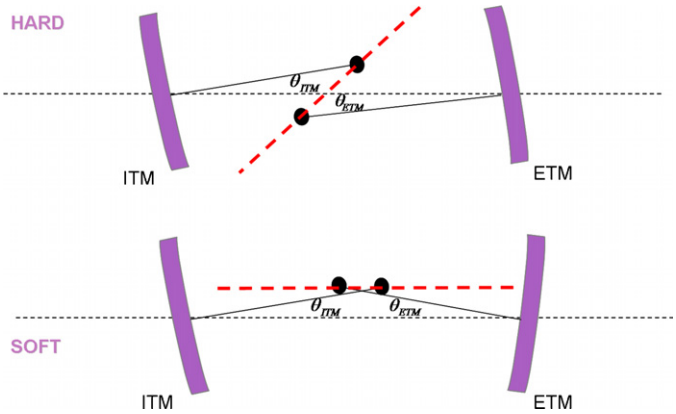

Figure 2. Representation of the basis which diagonalizes the torque stiffness matrix. Top: the hard mode; bottom: the soft mode.

Table 1. Suspension restoring torque and radiation pressure torque.

DOF	k_{res} (Nm)	I (kgm^2)	Radiation Pressure Torque	Value (Nm)
PITCH	9.72	0.757	k_S	−10.57
YAW	9.41	0.663	k_H	232.96

Using the terms in equation (4), the corresponding eigenvectors for the soft and hard modes are

$$v_S = [1, r] \qquad v_H = [r, -1], \tag{6}$$

with $r = 1.1533$ (appendix A). aLIGO will operate over a range of input powers. Since the torque induced by radiation pressure for the soft mode is negative, for each input power level its stability depends entirely on the restoring torque of the test mass suspension. We show in figure 3 the resonance frequency as a function of the power stored inside the arm cavities. When the power is low, the resonance frequencies of the two modes are equal to the nominal resonance frequency of the pendulum (around 600 mHz). The soft resonance moves to a lower frequency, while the frequency of the hard mode increases. The soft mode becomes unstable (corresponding to a negative resonance frequency) for arm cavity powers slightly lower than 700 kW, which is close to the maximum power planned for aLIGO.

The modification of the pitch opto-mechanical transfer functions due to radiation pressure in an aLIGO arm cavity can be seen in figure 4. In our model, the maximum circulating power in the aLIGO arm cavities is about 720 kW. The plot shows, in the case of a simple pendulum, the opto-mechanical transfer functions of the soft and hard mode in this regime, and the mechanical transfer function in absence of radiation pressure. As mentioned earlier, the soft mode is actually unstable. In order to make it stable, a special control filter needs to be designed. In particular, the unity gain frequency of the loop needs to be about 10 times higher than the frequency of the unstable resonance in order to provide overall stability.

2.3. Common and differential degrees of freedom

For an IFO like aLIGO, the error signals extracted from the IFO naturally distinguish between common and differential motions of the two cavities. It is therefore convenient to choose the

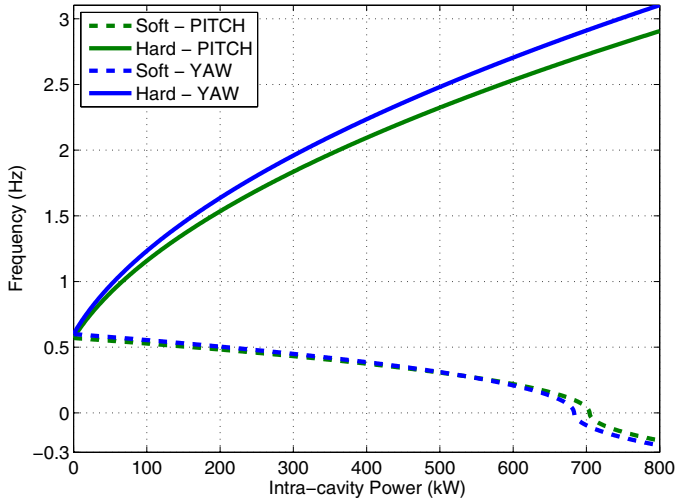

Figure 3. Frequency of the hard and soft modes for pitch and yaw in the aLIGO arm cavities, as a function of the intra-cavity power.

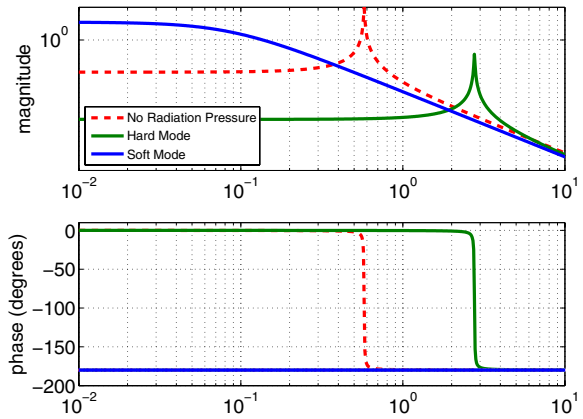

Figure 4. Opto-mechanical transfer functions for the hard and soft mode with 720 kW circulating inside the cavity. The dotted red curve shows the same transfer function in absence of radiation pressure.

basis of the common and differential soft and hard modes (see figure 5). The 4×4 matrix which expresses the misalignment of the cavity mirrors in terms of the new basis is

$$\begin{pmatrix} \theta_{\mathrm{EX}} \\ \theta_{\mathrm{EY}} \\ \theta_{\mathrm{IX}} \\ \theta_{\mathrm{IY}} \end{pmatrix} = \begin{pmatrix} 1 & r & 1 & r \\ 1 & r & -1 & -r \\ r & -1 & r & -1 \\ r & -1 & -r & 1 \end{pmatrix} \begin{pmatrix} \theta_{\mathrm{CommSOFT}} \\ \theta_{\mathrm{CommHARD}} \\ \theta_{\mathrm{DiffSOFT}} \\ \theta_{\mathrm{DiffHARD}} \end{pmatrix}. \tag{7}$$

The ASC model presented in the following section has been developed by adopting this particular choice of DOFs for the arm cavities, while for the other mirrors we consider the DOFs given by the simple misalignment of the mirrors. The arm cavity DOFs will be referred

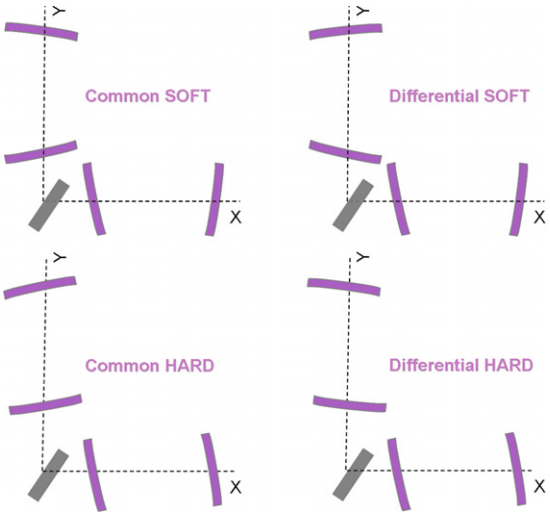

Figure 5. Soft and hard modes in common and differential combinations. The acronyms will be used in the rest of the paper to identify respectively the common soft (CS), differential soft (DS), common hard (CH) and differential hard (CH) DOFs.

to as CH, DH, CS and DS. For the other mirrors, the name of the mirror itself is used to refer to its misalignment: PRM, PR2, PR3, SRM, SR2, SR3, BS. Two additional degrees of freedom are given by the input beam orientation (both angle and position). Only the input beam angle (IN) is included here.

3. Alignment control for aLIGO

The fundamental requirement for the ASC scheme is to suppress the angular motion of the mirrors without reintroducing noise in the gravitational-wave signal, which is extracted at the asymmetric port of the IFO into the differential arm length signal (DARM). The angular motion has two fundamental contributors: seismic noise transmitted to the mirrors via their suspension systems and shot noise of the sensors transmitted to the mirrors via the control system itself[2]. These noises couple into DARM through a bilinear process in which residual beam spot motion (BSM) convolves with angular noise to produce a length signal. While the correct expression of this process is the convolution of the BSM spectrum with the angular noise spectrum, the fact that the BSM is predominantly at low frequency allows us to use the RMS of the BSM spectrum.

In this section, we describe the input noises of our model and the control loops designed for each degree of freedom in order to reduce the angular motion at low frequency, and to filter the noise reintroduced by the control system in the detection band. Finally, the performance of the ASC system is shown in terms of the noise coupling to DARM and the residual mirror motion. More details about the model architecture can be found in appendix B.

[2] Technical noises, such as electronic noise and acoustic noise, can also spoil the angular signals. In aLIGO, the alignment sensors will be placed under vacuum, so as to eliminate the noise coming from acoustic coupling, and the electronics has been re-designed to make the electronic noise well below the shot-noise level for each sensor.

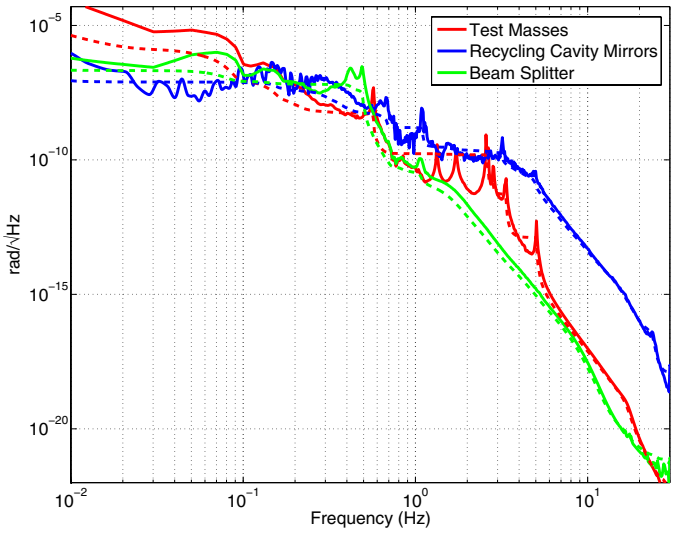

Figure 6. Angular pitch motion of all the IFO mirrors under local controls.

Table 2. Equivalent angle noise due to shot noise for each DOF. Units are 10^{-15} rad/$\sqrt{\text{Hz}}$. These values have been obtained by propagating the shot noise for each sensor through the input matrix (appendix B), and taking the incoherent sum of all the contributions for each DOF.

Unit	CS	CH	DS	DH	PRM	SR3	PR3	SRM	IN	BS
(10^{-15} rad/$\sqrt{\text{Hz}}$)	3.7	23	3.7	0.08	215	457	108	2134	339	18

3.1. Input noises: seismic noise and shot noise

The angular seismic noise of the optics used as input to this model is shown in figure 6. For each optic, an estimate of the pitch noise transferred to the mirrors has been made based on current measurements and models of the aLIGO suspensions [10–12]. A conservative estimate of the sensor noise of the local damping loops is made, and a longitudinal to pitch coupling due to locking forces on the test masses suspension chain is also present.

In aLIGO there will be two QPDs in transmission of each arm cavity in order to sense the dc position of the transmitted beam. Moreover, at least two WFSs will be located at each port of the IFO from which alignment RF error signals are planned to be extracted (REFL, AS, POP, see figure 1).

For each sensor, the limiting noise is assumed to be shot noise:

$$\widetilde{P}_{\text{Shot}} = \sqrt{2 \times h_P \times \nu \times P_{\text{dc}}} \quad \text{W}/\sqrt{\text{Hz}}, \tag{8}$$

where $h_P = 6.626 \times 10^{-34}$Js is Planck's constant, $\nu = 2.817 \times 10^{14}$ Hz is the frequency of the laser light and P_{dc} is the power impinging upon the diode. The power is assumed to be 50 mW for all the diodes, except for the ones at the AS port, where only 1% of the power is sent to the WFSs (resulting in about 2.5 mW on each diode).

The equivalent angular noise for each DOF due to shot noise is shown in table 2.

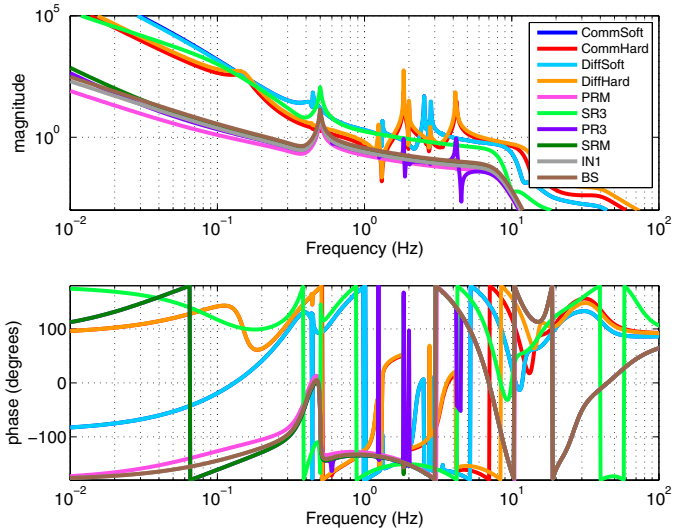

Figure 7. Open loop transfer functions of all the DOFs. The loops have been designed based on the opto-mechanical transfer functions of the system. In particular, a unity gain frequency of about 1.5 Hz is needed for the soft DOFs (naturally unstable) in order to provide overall stability.

3.2. Control loops

As shown in figure 6, the largest contribution to the mirror angular motion comes from low frequencies (below 1 Hz), so very high loop gain is needed in that frequency region. The control filters have been designed so as to have the lowest unity gain crossing of the common and differential soft loops around 1.5 Hz, at a frequency significantly higher than the unstable resonance frequency (80 mHz, see section 2.2). The lowest unity gain crossing of the hard modes of the cavities is a factor of 2 lower. The lowest unity gain crossing of the other loops is set between 100 and 200 mHz. The mechanical transfer functions of the aLIGO test mass suspensions are more complicated than that of a single pendulum, and they have been included in this model. Figure 7 shows the open loop transfer functions of all the DOFs.

3.3. Coupling to DARM

The angular noise coupled into DARM is computed by multiplying, for each mirror, the residual angular motion by the RMS of the BSM, and then summing over all the mirrors with their coupling coefficient to DARM. The BSM for each optic is shown in figure 8. For the test masses, the RMS is about 50 μm. The residual angular motion of some of the mirrors is shown in figure 9. The test masses have a residual angular motion of about 3 nrad, which agrees with the order-of-magnitude estimate given in [5].

Figure 10 is the most important figure of merit of the ASC scheme. It shows the contributions of the angular noise to DARM, coming both from the shot noise of the alignment sensors and the angular seismic noise of the mirrors. The aLIGO design sensitivity is plotted in black (dotted line). In the science mode, the target is to have the angular noise at least a factor of 10 below the sensitivity (in red, dotted line). The plot shows how the sum of the residual angular seismic noise of all the optics (in yellow) is well below the sensitivity.

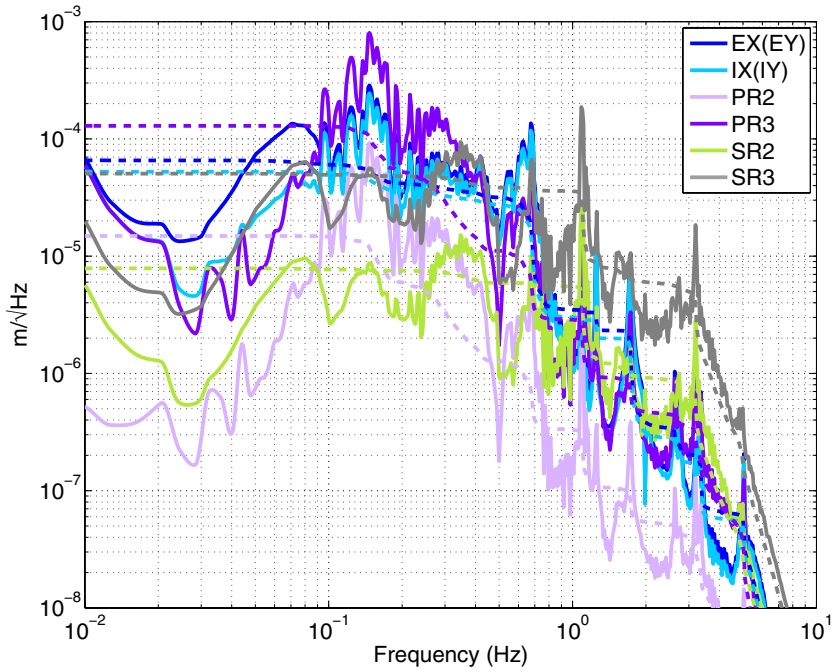

Figure 8. BSM for some of the mirrors. The two-end mirrors have a similar BSM (about 50 μm), as well as the two input mirrors. The BSM of the BS and the PR3 mirror is very similar. The dotted lines are the corresponding RMS.

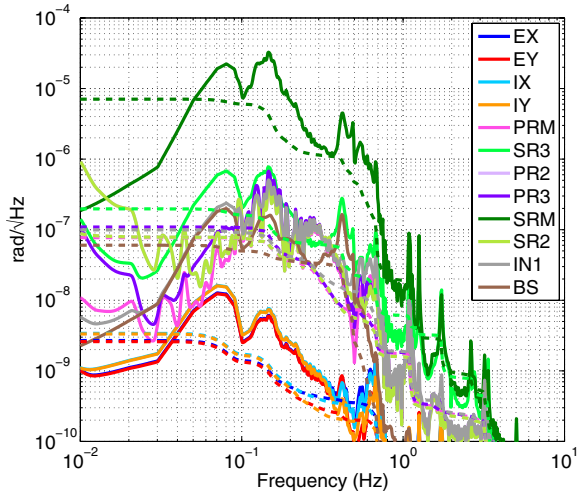

Figure 9. Residual pitch angular motion of each mirror. The dotted lines are the corresponding RMS. The RMS of the end mirror residual motion, for instance, is about 3 nrad.

Moreover, the total angular noise, which is mainly shot noise above 10 Hz, is well below the sensitivity in the detection band, and it meets the science-mode target above 15 Hz.

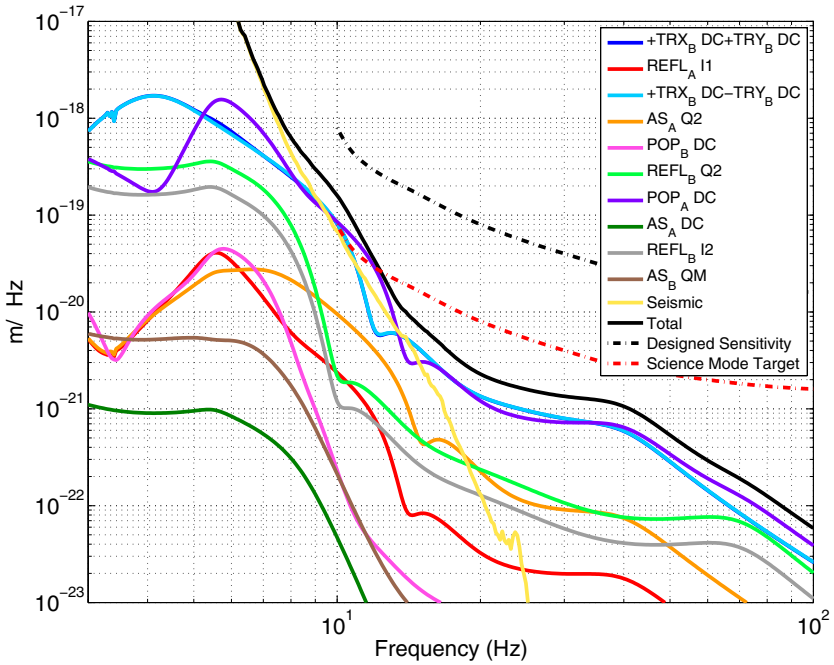

Figure 10. Angular noise coupling to DARM due to seismic noise (in yellow, sum over all the optics) and to shot noise (for each sensor).

4. Conclusions

The improvements in sensitivity which advanced LIGO will realize require a re-thinking of the alignment sensing and control scheme in order to properly deal with radiation pressure effects and sense all the important angular degrees of freedom of the IFO. We present a framework in which radiation pressure effects can be compensated in the control filters. From our results, we do not expect radiation pressure to compromise the controllability of the system. The shot noise of the sensors and the angular seismic noise of the mirrors are included in this model, and the angular noise coupling to the gravitational-wave channel is computed. The angular noise is compatible with science-mode operation of aLIGO.

Appendix A. Advanced LIGO parameters

The following tables summarize the aLIGO parameters considered in this model [13].

The g factors of the arm cavities are

$$g_{\mathrm{ETM}} = -0.7793 \tag{A.1}$$

$$g_{\mathrm{ITM}} = -1.0654 \tag{A.2}$$

The Gouy phases for the stable recycling cavities are

$$\phi_{\mathrm{PRC}} = 25^{\circ} \tag{A.3}$$

$$\phi_{\mathrm{SRC}} = 19^{\circ} \tag{A.4}$$

Table A1. Optical parameters of aLIGO.

Quantity	Value	Quantity	Value
Arm finesse	443	l_{PRC}	57.656 m
ITM transmission	1.4%	l_{SRC}	56.008 m
ETM transmission	5 ppm	l_{EX}, l_{EY}	3994.50 m
PRM transmission	3%	Lower mod. frequency (f1)	9099, 471 Hz
SRM transmission	20%	Upper mod. frequency (f2)	45, 497, 355 Hz
Schnupp asymmetry	0.05 m	Modulation index (f1, f2)	0.1

Table A2. Optical path distances between the HR surfaces of the optics (left) and ROC and beam size for each optic (right).

Distance	Value (m)	Optic	ROC (m)	Beam size (mm)
PRM $\longleftrightarrow$ PR2	16.6037	ETM	2245	62.0
PR2 $\longleftrightarrow$ PR3	16.1558	ITM	1934	53.0
PR3 $\longleftrightarrow$ BS	19.5384	PRM	−10.997	2.3
SRM $\longleftrightarrow$ SR2	15.726	PR2	−4.55	6.2
SR2 $\longleftrightarrow$ SR3	15.4607	PR3	36.00	54.0
SR3 $\longleftrightarrow$ BS	19.368	SRM	−5.6938	2.1
BS $\longleftrightarrow$ ITMX	5.3828	SR2	−6.428	8.2
BS $\longleftrightarrow$ ITMY	5.3328	SR3	36.00	54.0

Appendix B. Architecture of the ASC scheme

The architecture of the ASC scheme as developed in the model is described in figure B1. Each block corresponds to a matrix, while the white labels identify signal vectors. In the text, capitalization is used to identify the matrices which propagate the signal vector. Let us consider a vector $v_{MIRRORS}$ whose rows represent the angular motion of the mirrors. The angular motion of each optic causes the signals into the IFO to change according to the IFO response. If we build a vector $v_{SENSORS}$ in which each row corresponds to one of the signals of the IFO used in the ASC scheme, the signals can be combined through an "INPUT MATRIX" to define a vector v_{ERROR} of signals which sense the angular degrees of freedom of the IFO. The error signals are filtered by the "CONTROL FILTERS" matrix, and the resulting vector $v_{CONTROL}$ is mapped to a vector v_{CORR} of correction signals, which are then filtered to take into account the particular mirror response and sent to the actuators. The mechanical "PENDULUM RESPONSE" translates the actuation force to angular motion of the "MIRRORS". The matrices which define the model are built in the following way:

- the Optickle model provides the transfer functions which simulate the "IFO Optical Response";
- the "Input Matrix" has to be computed in order to reconstruct the error signals of the angular DOFs;
- the "Control Filters" and "Mirror Compensators" are designed to obtain the desired performance;
- the common and differential hard and soft matrix described in section 2.3 defines the angular DOF basis which diagonalizes the torque stiffness matrix in the presence of radiation pressure ("DOF map to MIRROR");
- the pendulum response is based on precise models of the aLIGO suspensions [12].

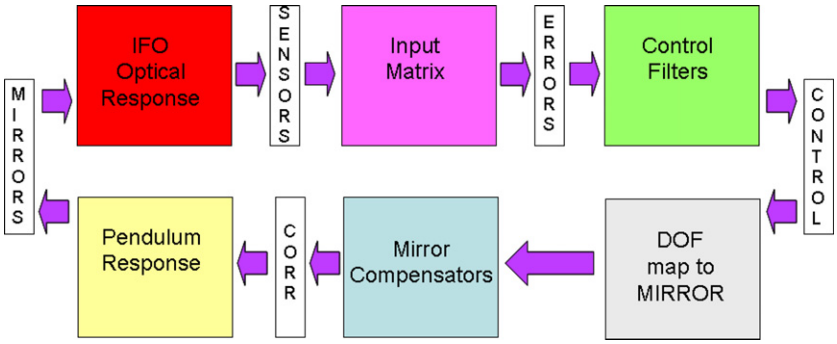

Figure B1. Architecture of the ASC model. The colorful blocks correspond to matrices, while the white labels correspond to signal vectors.

Computation of the input matrix and control filters design will be detailed in the following subsections. The model has been developed only for the pitch angular DOFs, but similar results are expected for yaw.

B.1. Input matrix

A general reconstruction of the angular DOFs of the IFO would come from a frequency-dependent "Input Matrix". The DOF to mirror mapping is chosen such that it diagonalizes the frequency dependence of the IFO response, making the product equivalent to a diagonal-frequency-dependent matrix (compensated in the "CONTROL FILTERS") times a frequency-independent sensing matrix, which can be directly computed by calculating the response in the error signal to a motion of the angular DOFs. The input matrix is an approximation to the inverse of the sensing matrix, and it can be, therefore, computed only at a single frequency.

The sensing matrix is given by the sensitivity of the signals extracted from the IFO to the motion of the degrees of freedom of the system. The suffixes used to identify the two detectors at each port are A and B. The letters I and Q are used to identify the in-phase and quadrature-phase signals from the WFSs. The demodulation frequencies (listed in appendix A) are written as 1 (f1), 2 (f2) or M (f2 - f1). On the basis of the signal sensitivity to the IFO DOFs, the Gouy phases have been set as shown in table B.1:

Port	Sensor	Gouy Phase (dg)	$A\angle B(dg)$
TRX, TRY	*A*	14	90
	B	−76	
AS	*A*	23.7	100
	B	122.5	
REFL	*A*	147.2	90
	B	57.2	
POP	*A*	139.1	60
	B	78.7	

(B.1)

The demodulation phases of the RF signals have been set in order to maximize the sensitivity to the given DOF in I for the common signals and in Q for the differential ones, as shown in table B.2:

Sensor	Demdd frequency	Demod phase (dg)
AS_B	fM	166.2
AS_A	$f2$	117.1
REFL_A	$f1$	−17.5
REFL_B	$f2$	−85.1

(B.2)

The sensitivity of the selected signals with respect to the IFO DOFs is shown in the sensing matrix (spanning tables B.3 and B.4), where all the amplitudes are in W/mrad. The common and differential signals for the arm cavity soft modes are the sum and the difference of the transmitted dc signals TRX_dc and TRY_dc.

Signals/DOFs	CS	CH	DS	DH	PRM	PR2
TR_dcComm	**−36.4**	0.3	0.4	0	0	0
REFL_AI1	**−37.8**	**−211.8**	−0.4	0.4	1.6	5.3
TR_dcDiff	0.4	0	**−36.4**	−0.2	0	0
AS_AQ2	1.4	−1.3	23.0	**374.6**	0	0
POP_Bdc	1.4	**35.1**	0	−0.1	−0.7	0
REFL_BQ2	**−0.6**	**−0.4**	**−1.0**	**0.9**	**0.4**	0.1
POP_Adc	4.0	**91.1**	0.1	−0.1	−0.4	0.1
AS_Adc	−2.7	2.4	−21.4	**−237.5**	0	0
REFL_BI2	**0.8**	**−4.6**	−0.4	0.4	**0.6**	−0.2
AS_BQM	0	0	**2.7**	**−2.3**	0	0

(B.3)

Signals/DOFs	PR3	SRM	SR2	SR3	IN1	BS
TR_dcComm	−0.1	0	0	0	0	0
REFL_AI1	**45.3**	0	0	0	0.2	15.5
TR_dcDiff	0	0	0	0	0	0
AS_AQ2	0	0	−0.4	−2.5	0	2.9
POP_Bdc	0.6	0	0	−0.0	0	0.2
REFL_BQ2	**0.6**	0	0.1	**0.5**	**−0.4**	**−0.6**
POP_Adc	1.3	0	0	0	0	0.5
AS_Adc	0	0.1	0.7	4.8	0	−7.0
REFL_BI2	**−1.8**	0	0	0	**−0.7**	**−0.9**
AS_BQM	0	0	0	0	0	**1.7**

(B.4)

Matrices B.3 and B.4 show that all the signals are dominated by the arm cavity motion. In order to suppress their large error signals and to be able to extract the DOFs of the recycling cavities, the arm cavity loops have much more gain at low frequency than the other loops: the bandwidths of the arm cavity loops are about 1 Hz, while the bandwidth of the other loops is roughly 100 mHz. Among the power and signal recycling cavity optics, only SR3 is controlled with a bandwidth approaching 1 Hz (see figure 6).

With this gain hierarchy, the input matrix which reconstructs the error signals for the DOFs in mrad/W is the following:

	TR Comm	REF A I1	TR Diff	AS A Q2	POP B dc	POP A dc	AS A dc	REF B Q2	REF B I2	AS B QM
CS	**−0.03**	−0	0	0	0	0	0	0	0	0
CH	0.005	−0.005	0	0	0	**0.17**	0	0	0	0
DS	0	0	**−0.03**	0	0	0	0	0	0	0
DH	0	0	0	**0.003**	0	0	0	0	0	0
PRM	0	0	0	0	**−1.41**	**0.70**	0	0	0	0
PR3	0	0	0	0	0	**0.79**	0	0	0	0
SRM	0	0	0	0	0	0	**10.81**	−0	0	**45.32**
SR3	−0.03	−0.004	−0.06	−0.005	0.06	**−2.41**	0	**2.05**	**−1.11**	0.14
IN1	0	0	0	0	**−1.32**	**−1.48**	0	0	**−1.48**	**−0.80**
BS	0	0	0	0	0	0	0	0	0	**0.60**

(B.5)

Note that in this ASC scheme the SR2 and PR2 mirrors are not globally controlled. The main reason is that the angular motion of these optics coupled to DARM is already below the sensitivity curve (see figure 10, where the sum of the angular seismic noise of all the optics is shown in yellow).

References

[1] Abbott B P *et al* 2009 LIGO: the Laser Interferometer Gravitational-Wave Observatory *Rep. Prog. Phys.* **72** 076901

[2] Accadia T 2010 *Class. Quantum Grav.* **27** 084002

[3] Grote H (for the LIGO Scientific Collaboration) 2010 *Class. Quantum Grav.* **27** 084003

[4] Harry G (for the LIGO Scientific Collaboration) 2010 *Class. Quantum Grav.* **27** 084006

[5] Mueller G 2005 Beam jitter coupling in advanced LIGO *Opt. Express* **13** 7118–32

[6] Fritschel P *et al* 1998 Alignment of an interferometric gravitational wave detector *Appl. Opt.* **37** 28

[7] Ballmer *et al* 2007 Advanced LIGO interferometer sensing and control conceptual design document *LIGO Internal Note* LIGO-T070247

[8] Optickle is available in the MIT CVS repository at emvogil-3.mit.edu:/export/cvs/iscmodeling

[9] Sidles J and Sigg D 2006 Optical torques in suspended Fabry–Perot interferometers *Phys. Lett.* A **354** 167–72

[10] Matichard F *et al* 2009 it Advanced LIGO preliminary design review of the BSC ISI system *LIGO Internal Document* LIGO-L0900118

[11] Kissel *et al* 2009 L1 HAM6 ISI eLIGO final performance measurements *LIGO Internal Document* LIGO-T0900285-v1

[12] Shapiro B 2009 personal communication

[13] Arain M and Mueller G 2009 Optical layout and parameters for the advanced LIGO cavities *LIGO Internal Document* LIGO-T0900043-08